Environmental Science Advances

ROYAL SOCIETY OF CHEMISTRY

PAPER

View Article Online
View Journal | View Issue

Open Access Article. Published on 30 September 2024. Downloaded on 10/24/2025 11:24:44 PM.
This article is licensed under a Creative Commons Attribution-NonCommercial 3.0 Unported Licence.

Check for updates

Cite this: *Environ. Sci.: Adv.*, 2024, **3**, 1722

Lignin cationization for the removal of phosphates and nitrates from effluents of wastewater treatment plants†

Fannyuy V. Kewir,[a] Carlos E. Astete,[a] Divine B. Nde,[b] Jessica R. Eberhard,[c] W. David Constant[a] and Cristina M. Sabliov *[a]

The removal of phosphates and nitrates from wastewater treatment plant (WWTP) effluents is important for preventing pollution of receiving waters. In this study, we chemically modified alkaline lignin (aLN) with quaternary ammonium groups to obtain biodegradable cationic lignin (cLN). We characterized the cLN and tested its efficacy for removing phosphates and nitrates in a lab setting and on field-collected WWTP samples. Adsorption isotherm and kinetic studies were performed in aqueous media, and the effects of several variables (contact time, pH, initial concentration, and adsorbent dose) were investigated. The Langmuir isotherm described phosphate and nitrate adsorption well, with R^2 values of 0.97 and 0.84, and maximum adsorption capacities of 0.59 mg g^{-1} and 2 mg g^{-1} respectively. For phosphate, the data fit the Freundlich isotherm model with an R^2 of 0.95, suggesting that both homogenous and heterogeneous adsorbent surfaces were involved in phosphate adsorption. Adsorption kinetics revealed that both phosphate and nitrate sorption onto cLN was better described by the pseudo-second-order model, with a correlation coefficient of 1. Furthermore, a 2-dimension Doehlert matrix was used to model the effect of initial concentration and adsorbent dose on the phosphate and nitrate removal. The results showed that cLN 1516 mol% was most effective for low phosphate and nitrate concentrations. With an obtained optimum adsorbent dose of 10 mg mL^{-1}, we achieved a successful reduction of nutrient loads of WWTP effluent from 0.42 mg L^{-1} to 0.18 mg L^{-1} (adsorption capacity of 0.6 mg g^{-1}) and from 4.1 mg L^{-1} to 2.3 mg L^{-1} (adsorption capacity of 4.5 mg g^{-1}), corresponding to the removal of 57.7% and 43.9% for phosphates and nitrates respectively.

Received 9th August 2024
Accepted 29th September 2024

DOI: 10.1039/d4va00312h

rsc.li/esadvances

Environmental significance

The research paper "Lignin cationization for the removal of phosphates and nitrates from effluents of wastewater treatment plants" addresses the important problem of water pollution from a point source. Our approach involved repurposing a waste stream from the paper and pulp industry, lignin, to reduce the nutrient loads of final effluents of wastewater treatment plants. This approach was intended to follow and close the circular economy loop whereby waste material is used for environmental remediation with the potential for application as phosphate and nitrate fertilizer for plants.

1. Introduction

Water treatment is a key component of sustainable water resource management. However, wastewater treatment plants (WWTPs) constitute a major point source of pollution, with effluent loads often greater than those of nonpoint sources.[1] Nitrates and phosphates are among the pollutants present in the water taken in by WWTPs and originate from various sources, including agricultural, industrial, and household waste.[2,3] The efficient removal of these pollutants before the release of WWTP effluents into the natural environment is important, since high phosphorus and nitrogen concentrations (between 20–100 and 500–1000 μg L^{-1} respectively) can cause excessive algal and plant growth, leading to eutrophication in aquatic habitats.[4] An increase in mortality of aquatic life due to eutrophication causes an imbalance of aquatic ecosystems while the continued supply of nutrient loads upsets the biogeochemical cycles of nitrogen and phosphorus.[5] In this regard, the United States Environmental Protection Agency (USEPA) has set strict ecoregion-specific concentration ranges for total nitrogen (0.12–2.18 mg L^{-1}) and total phosphorus

[a]Biological & Agricultural Engineering Department, Louisiana State University, LSU Ag Center, Baton Rouge, Louisiana 70803, USA. E-mail: csabliov@lsu.edu

[b]Department of Chemistry, Louisiana State University, Baton Rouge, Louisiana 70803, USA

[c]Department of Biological Sciences, Museum of Natural Science, Louisiana State University, Baton Rouge, LA 70803, USA

† Electronic supplementary information (ESI) available. See DOI: https://doi.org/10.1039/d4va00312h

© 2024 The Author(s). Published by the Royal Society of Chemistry

Open Access Article. Published on 30 September 2024. Downloaded on 10/24/2025 11:24:44 PM.
This article is licensed under a Creative Commons Attribution-NonCommercial 3.0 Unported Licence.

(0.076–0.1 mg L^{-1}) on WWTPs, to reduce effluent nutrient concentrations and protect receiving waters.[1]

Biological and chemical methods have been researched and implemented for wastewater treatment, but their use is often limited due to high costs and instability.[6] Adsorption is generally preferred to chemical (such as precipitation with iron salts, alum, or lime) and biological (aerobic and anaerobic) treatments due to convenience, flexibility, ease of operation, simplicity of design, and reduced production of sludge.[2,7,8] Metal-based adsorbents and composite materials are some conventional adsorbents that have been utilized with some success but they have drawbacks such as low sorption capacity, limited surface area/active sites, and short adsorption–regeneration cycles.[9] Activated carbon has proven to be an effective adsorbent but its high cost limits large-scale use.[10,11] In recent years, research has been oriented toward finding cheaper, more efficient, and sustainable adsorbent materials, with a great deal of this research focused on lignin-based materials.[12]

Lignin is the second most abundant biopolymer on Earth[13] after cellulose. It exhibits several characteristics such as biodegradability/biocompatibility, aromaticity, high thermal stability, renewability, easy functionalization, durability, and low cost[12,14,15] that make it attractive for the synthesis of biomaterials. Lignin contains a large number of active functional groups such as aliphatic and phenolic hydroxyl groups, carbonyl groups, methoxy groups, and phenyl groups,[16] which make it suitable as a chelating agent for a variety of contaminants in water/wastewater.[12] Lignin functionalization and chemical and physical modification have received a great deal of attention in efforts to increase its efficiency as a removal agent for wastewater applications. Although a considerable amount of research has been conducted on the use of lignin-based materials as adsorbents for removing heavy metals, dyes, and sulfates,[12,13,16–23] fewer studies[23,24] have explored the ability of raw lignin to remove phosphates and nitrates from wastewater. After experimenting with phosphate and nitrate removal using lignin, Sajjadi's work[12] suggested that the ineffectiveness of lignin may be due to its coiled 3D structure and overall negative charge, which would induce double-layer electrostatic repulsion with the phosphate and nitrate anions during adsorption.

Because adsorption is a surface phenomenon, the efficiency of the process is intrinsically tied to adsorbent properties such as surface charge and surface area. A large surface area provides maximum available sites for interaction, thereby increasing adsorption capacity. Both Zong's[23] and Li's[13] groups demonstrated the capability and versatility of lignin-based adsorbents for contaminant removal from wastewater. However, like the materials they used, the literature reveals that the focus has been on inorganic composites with components (for example, positively charged polyethylenimine) that may be toxic to the environment due to their potential for bioaccumulation and environmental persistence. Moreover, some of these adsorbents are non-recyclable.

In this study, we designed a positively charged biodegradable lignin polymer for improved phosphate and nitrate removal and with potential recyclability through agricultural applications. We adopted a circular economy approach, wherein biodegradable lignin was derived from waste biomass, chemically modified, and used in environmental remediation, leaving a minimal environmental footprint. The circular economy can be defined as a system that is restorative or regenerative by intention and design, replacing the 'end-of-life' concept and aiming to eliminate waste and the use of toxic chemicals that impair reuse. These goals are met through the superior design of materials, products, and systems.[25] Specifically, we chemically modified alkaline lignin (aLN) with quaternary ammonium groups following methods previously studied by Chauhan *et al.*, Gogoi *et al.*, and Pinto *et al.*[26–28] to modify biomass. The resulting cationic lignin (cLN) was tested in a laboratory setting and on field-collected WWTP samples, as a novel biobased system[29] for the adsorption of phosphates and nitrates from aqueous media. Following chemical characterization of the cLN, we performed isotherm and kinetic studies in batch adsorption experiments and investigated the effects of several variables (contact time, pH of the solution, initial ion concentration, competing anions, and adsorbent dose) on adsorption efficacy. To our knowledge, the materials synthesized and tested in this study have not previously been used for phosphate and nitrate removal.

2. Materials and methods

2.1. Materials

The alkaline lignin used was purchased from TCI (Portland, OR), sodium hydroxide (NaOH) and hydrochloric acid (HCl) were supplied by VWR International (West Chester, PA), and sulfuric acid (H_2SO_4) was purchased from Ricca Chemical Company (Arlington, TX). Glycidyl triethylammonium chloride (GTAC), poly[lactic-*co*-glycolic acid] (PLGA), oxalyl chloride, Amicon Ultra 0.5 mL centrifugal filters and 2-chloro-4,4,5,5-tetramethyl-1,3,2-dioxaphospholane (TMDP) were purchased from Sigma Aldrich (St. Louis, MO). Anhydrous dimethyl sulfoxide (DMSO) was purchased from Alfa Aesar (Ward Hill, MA) while regular DMSO was from Thermo Fisher Scientific (Waltham, MA). Dichloromethane (DCM), dimethylformamide (DMF), pyridine, chloroform-d, chromium(III) 2,4-pentanedionate ($Cr(acac)_3$), cyclohexanol, potassium dihydrogen phosphate (KH_2PO_4), ammonium molybdate ($(NH_4)Mo_7O_{24}\cdot 4H_2O$), potassium antimonyl tartrate trihydrate ($K(SbO)C_4H_4O_6\cdot 1/2H_2O$), ascorbic acid, and sodium nitrate ($NaNO_3$) were also purchased from Thermo Fisher Scientific (Waltham, MA), while NitraVer X nitrate reagent set and test 'N Tubes' were supplied by HACH Company (Loveland, CO, USA). All solutions were prepared with deionized water DI H_2O (resistivity 18.2 MΩ cm, Millipore, Milli-Q, Barnstead International, Dubuque, IA).

2.2. Synthesis of cationic lignin

The cationic synthesis protocol was adapted from Kong's[30] and Wahlström's[20] works. Briefly, 2 g of lignin was dissolved in 100 mL of DI H_2O (DI H_2O; resistivity 18.2 MΩ cm, Millipore, Milli-Q, Barnstead International, Dubuque, IA) and the pH was adjusted to 12.5 using a 0.2 M NaOH solution. The solution was

Open Access Article. Published on 30 September 2024. Downloaded on 10/24/2025 11:24:44 PM.
This article is licensed under a Creative Commons Attribution-NonCommercial 3.0 Unported Licence.

then transferred to a 250 mL three-neck round-bottom flask and placed in an oil bath at 60 °C and 220 rpm. Next, we added glycidyl triethylammonium chloride (GTAC) to the lignin at volumes corresponding to the desired mol percent dosages. After 24 h, the solution was submerged in a cold-water bath for 30 min and then transferred into dialysis tubing (MWCO 12–14 kD), and submerged in deionized water for 48 h to remove any unreacted GTAC and other impurities. The dialysis water was replaced every 6 h for 48 h. After dialysis, the solution containing the cationic lignin was freeze-dried (Labconco, MO, USA), and the samples were stored at −20 °C for further analysis.

2.3. Characterization of cationic lignin

The amounts of various OH groups (aliphatic-OH, carboxylic-OH, and phenolic-OH [*para*-OH phenyl, condensed and syringyl-OH, guaiacyl-OH, and catechol-OH groups]) in the unmodified and cLN, lignin were estimated using ^{31}P NMR after phosphitylation with 2-chloro-4,4,5,5-tetramethyl-1,3,2-dioxaphospholane (TMDP), as described in various published protocols (*e.g.*, ref. 31–33). The chemical shift ranges integrated for various OH group types in the quantification of lignin substructures were adapted from Araneda.[34] We estimated the degree of substitution (DS) as the ratio of substituted phenolic-OH groups (original minus derivatized amounts of OH groups given by ^{31}P NMR spectra) divided by the original number of OH groups.[20]

We measured the zeta potential of our synthesized cLN dispersed in DI H_2O using a PMX-430 ZetaView QUATT Laser analyzer (Particle Matrix, Ammersee, Germany). A Zetasizer Nano ZS (Malvern Instruments, Malvern, UK) was used to obtain the point of zero charges of the cLN by titrating NaOH solutions against the cLN and observing the variation of zeta potential with pH and size.[20]

We obtained FT-IR spectra in the range of 4000–400 cm^{-1} by the attenuated total reflectance (ATR) method at room temperature using a spectrometer (Bruker Alpha P, Germany). We acquired scanning electron microscope (SEM) images and elemental mapping by energy dispersive X-ray spectrometry (SEM/EDS) using a JSM-6700F (JEOL Ltd, Tokyo, Japan) of cLN that had been sputter-coated with a thin layer of platinum.

2.4. Phosphate and nitrate adsorptions

The adsorption capacity of the synthesized cLN was evaluated in a batch system. Using a protocol adapted from Jiao[35] and Zong.[23] 100 mg L^{-1} stock phosphate and nitrate solutions were prepared by dissolving 143.25 mg of KH_2PO_4 and 137.10 mg respectively, in DI water and diluted accordingly to obtain the desired concentrations. Each adsorption experiment was done with an adsorbent dose of 2 mg L^{-1} at room temperature and a stirring speed of 300 rpm. The pH was maintained at neutral pH. The samples were centrifuged using a JXN-26 centrifuge (Beckman Coulter Inc., CA, USA) at 11 000 rpm and 10 °C for 30 min and collected in 2 mL Amicon Ultra 0.5 centrifugal filter tubes. The ion concentrations of the filtrate were determined as described in Section 2.6. For each experimental run, the amount of adsorbate per unit weight of adsorbent at time t, q_t (mg g^{-1}), was calculated according to eqn (1):

$$q_t = (C_0 - C_t)V/m \tag{1}$$

where C_0 and C_t (mg L^{-1}) are the concentrations of the phosphate and nitrate at times t_0 and t respectively; V (mL) is the volume of the solution, and m (g) is the weight of the adsorbent used.

The sorption percentage was estimated from eqn (2):

$$\text{Sorption (\%)} = (C_\text{i} - C_\text{e})/C_\text{i} \times 100 \tag{2}$$

where C_i and C_e are the initial and equilibrium concentrations of the ions of interest (*i.e.*, phosphates and nitrates).

To investigate the effects of the adsorbent dose and initial ion concentration on the removal percentage, a 2-factor Doehlert's matrix was used to plan the experiments and optimize the process.[36,37] For 2 factors, the Doehlert design consists of seven experiments comprising a central point (0) and six others represented in a coded value matrix (Table 1). Adsorption experiments were carried out at room temperature with an agitation speed of 300 rpm, pH 7, and contact time of 25 min. Aliquots of 1.5 mL were withdrawn from the mixture at predetermined time intervals and centrifuged using a JXN-26 centrifuge (Beckman Coulter Inc., CA, USA) at 11 000 rpm and 10 °C for 30 min. The resulting supernatant was used to determine the phosphate and nitrate concentrations. These experiments were carried out in duplicates.

For this design, Lagrange's criterion for the two-variable function was used to model the response (eqn (3)):

$$Y = a + b(X_1) + c(X_2) + d(X_1^2) + e(X_2^2) + f(X_1X_2) \tag{3}$$

where Y is the experimental response to be optimized; a is a constant term; b and c are coefficients of the linear terms; d and e are coefficients of the quadratic terms; and f is the coefficient of interaction between the two variables,[36] which were determined through linear regression analysis.

As a realistic test of the adsorption capacity of our adsorbent, we conducted adsorption experiments as described above using final effluent samples from one WWTP in Baton Rouge, LA, USA; South Baton Rouge (SBR) plant. Samples were collected in 1 liter bottles and stored in an ice chest with ice while being transported from the plants to the lab. After filtration with a P8

Table 1 2-parameter Doehlert matrix experimental design

	Coded variables	
Expt #	X_1	X_2
1	0	0
2	1	0
3	−1	0
4	0.5	0.866
5	−0.5	−0.866
6	0.5	−0.866
7	−0.5	0.866

 © 2024 The Author(s). Published by the Royal Society of Chemistry

Open Access Article. Published on 30 September 2024. Downloaded on 10/24/2025 11:24:44 PM.
This article is licensed under a Creative Commons Attribution-NonCommercial 3.0 Unported Licence.

qualitative filter paper (Fisher Scientific, Pittsburgh, PA), we tested the samples for the presence of phosphates and nitrates as described in Section 2.6, and carried out adsorption experiments using optimum adsorption conditions that were selected based on the initial lab experiments described above.

2.5. Adsorption kinetics and isotherm models

Kinetic models and adsorption isotherms are often used to assess the efficiency and adsorption capacity of adsorbent material. The most commonly used isotherms are the linear Langmuir and Freundlich models.[38] We determined the linear Langmuir and Freundlich adsorption isotherms by varying the initial concentrations[38] of phosphate (from 0.5 to 1 mg L^{-1}) and nitrates (3.6 to 15.8 mg L^{-1}) by diluting the stock solutions accordingly; we used an adsorbent dose of 2 mg mL^{-1} with a contact time of 90 min at room temperature and neutral pH. The linear Langmuir model, which can be used to describe adsorbate–adsorbent interaction at the solid–liquid (monolayer) interface,[4] is summarized by eqn (4):

$$\frac{C_e}{q_e} = \frac{1}{q_{maxL} K_L} + \frac{C_e}{q_{max}} \tag{4}$$

where q_e is the amount of adsorbate adsorbed (mg g^{-1}), C_e is the equilibrium concentration of adsorbate solution after adsorption (ppm), q_{max} is the Langmuir adsorption capacity, and K_L (L mg^{-1}) is the Langmuir constant. The dimensionless separation constant R_L, defined by eqn (5), describes the nature of adsorption as unfavorable ($R_L > 1$), linear ($R_L = 1$), favorable ($0 < R_L < 1$), or irreversible ($R_L = 0$):[4,39–41]

$$R_L = \frac{1}{1 + K_L C_0} \tag{5}$$

where C_0 is the initial adsorbate concentration (ppm).

The linear Freundlich model, which describes multilayer sorption (chemisorption) on heterogeneous surfaces,[40] is described by eqn (6):

$$\ln q_e = \ln K_F + \frac{1}{n} \ln C_e \tag{6}$$

where K_F is the Freundlich constant, n is the heterogeneity factor related to the adhesion of the adsorbate to the adsorbent surface, and $n > 1$ indicates favorable adsorption.[38,40] The slope and intercept of the linear regression of $\ln C_e$ to $\ln q_e$ are used to determine n and K_F.

The linearized pseudo-first- and second-order (PFO and PSO) expressions are described by eqn (7) and (8) respectively:

$$\ln(q_e - q_t) = \ln q_e - K_1 t \tag{7}$$

$$\frac{t}{q_t} = \frac{1}{K_2 q_e^2} + \frac{t}{q_e} \tag{8}$$

where K_1 (min^{-1}) and K_2 (g (mg min^{-1})$^{-1}$) are the rate constants.

2.6. Determination of phosphate and nitrate concentration

To measure the concentration of phosphates in our samples, we adapted a protocol used with an automatic AQ300 Discrete Analyzer (SEAL Analytical). The original protocol is equivalent to USEPA Method 365.1, Rev 2.0, and is approved for the Clean Water Act (CWA) for use in wastewater compliance monitoring under the National Pollutant Discharge Elimination System (NPDES). Our modified protocol was used to conduct the analyses manually and phosphate concentrations reported refer to orthophosphate–phosphorus (PO_4–P).

We prepared five different stock solutions using DI water: 2.5 M H_2SO_4, a 4% (w/v) ammonium molybdate (CAS: 12054-85-2) solution, a 3 g L^{-1} potassium antimonyl tartrate trihydrate (CAS: 28300-74-5) solution, and a 15 g L^{-1} ascorbic acid (CAS: 50-81-7) solution spiked with 0.12 mg P/L standard. With these reagents, we prepared a working phosphate color reagent using the following proportions: 65 mL (2.5 M H_2SO_4) + 22 mL (4% w/v ammonium molybdate) + 7.5 mL (3 g L^{-1} potassium antimonyl tartrate trihydrate), brought to 100 mL with DI water. We added 140 μL of the color reagent and 40 μL of ascorbic acid to 400 μL of the sample. After an 8 minute reaction time to allow for the color change (reduced phosphomolybdate blue complex formation) to occur, we placed 200 μL of the mixture in a well plate. We then measured light absorbance at a wavelength of 880 nm using a BioTek Cytation 3 plate reader photo spectrometer (BioTek Instruments Inc., VT, USA). We generated and used a phosphate standard curve to estimate orthophosphates in subsequent adsorption studies.

Nitrate concentrations were tested according to the nitrate chromotropic acid TNT method using a DR-900 colorimeter (HACH Company, Loveland, CO, USA) at 420 nm. Nitrate concentrations reported refer to nitrate–nitrogen (NO_3^-–N).

3. Results and discussion

3.1. Lignin chemical modification/structure confirmation

Commercial alkaline lignin (TCI America) was used for cationization and further analyses. The cationization was done following various GTAC dosages calculated based on the total

Table 2 Estimated OH groups in uncationized and cationized lignins

GTAC vol. (mL)	GTAC dosage (mol%)	Aliphatic OH (mmol g^{-1})	Phenolic OH (mmol g^{-1})	COOH (mmol g^{-1})	Zeta potential (mV)	pH
0.0	0.0	1.5 ± 0.4	2.3 ± 0.7	0.7 ± 0.3	−44.0	2.3
3.2	461.0	2.2 ± 0.4	0.8 ± 0.0	0.5 ± 0.1	−15.0	7.1
3.5	505.5	2.3 ± 0.1	0.4 ± 0.1	0.4 ± 0.0	−9.9	6.7
5.3	768.3	2.3 ± 0.9	0.7 ± 0.3	0.4 ± 0.2	−7.8	6.8
6.4	922.0	2.0 ± 1.1	0.5 ± 0.2	0.4 ± 0.2	6.4	7.0
10.5	1516.5	1.1 ± 0.7	0.2 ± 0.1	0.2 ± 0.1	18.5	6.8

Open Access Article. Published on 30 September 2024. Downloaded on 10/24/2025 11:24:44 PM.
This article is licensed under a Creative Commons Attribution-NonCommercial 3.0 Unported Licence.

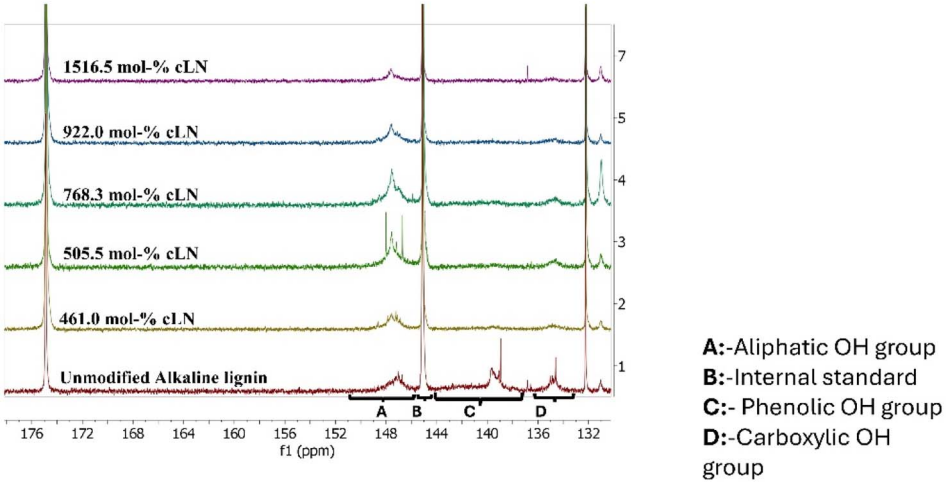

Fig. 1 Stacked ^{31}P NMR spectra of uncationized and varied degrees of cationized lignin.

initial number of phenolic-OH groups in the uncationized lignin. The alkaline lignin had a total phenolic OH group of 2.32 mmol g^{-1} (see Table 2) and was rich in guaiacyl units (1.30 mmol g^{-1}) with fewer syringyl units (0.29 mmol g^{-1}). Hence, it can be concluded that the lignin source (not specified by the company, TCI America) is softwood lignin. However, within the circular economy framework, it would be advisable to use hardwood (not softwood) waste biomass as source material for lignin extraction because it contains a higher proportion of phenolic OH groups, in particular syringyl units with methoxy groups that are susceptible to modification, specifically cationization in our case.

3.2. Characterization of cationic lignin

3.2.1. OH-groups in uncationized and cationized lignin. After the alkaline lignin cationization, ^{31}P NMR (Fig. 1) was used to estimate the amount of aliphatic-, reactive phenolic-, and carboxylic-OH groups with spectra integrated over chemical shift ranges of 150.0–145.4 ppm, 144.5–137.0 ppm, and 136.0–133.6 ppm, respectively.

The variation in the peak intensities of the various OH groups, for both the unmodified and cLN, is illustrated in the stacked ^{31}P NMR spectra (Fig. 1), for sections of the spectra that correspond to those OH groups. The variation observed with the OH-group types quantified in mmol g^{-1} (up to a 1516 mol% dosage) was consistent with published studies, with an increase in the aliphatic-OH groups due to the opening of the epoxy ring,[20] a decrease in the phenolic-OH groups, and only a slight reduction of carboxylic-OH groups with varied GTAC dosage.

Estimated amounts of the various OH groups in the lignin modifications are summarized in Table 2. The observed reduction in the amount of phenolic-OH groups with GTAC dosage confirms that the reaction site for the substitution by the quaternary ammonium salt of GTAC was the phenolic group of lignin. This agrees with Kong *et al.*[30] (2015) and Acurio Cerda *et al.*[42] (2023). After this series of chemical modifications, the zeta potentials were determined (Table 2). The 922 and 1516 mol% cLN were chosen for further testing because of their positive zeta potentials at ≈neutral pHs. ALN was used as a control in adsorption studies.

The variation of zeta potential with pH of cLN 922 and 1516 was used to determine the points of zero charge (pH_{pzc}). For cLN 922, the zeta potential ranged from +31.6 mV at pH 2.3 to

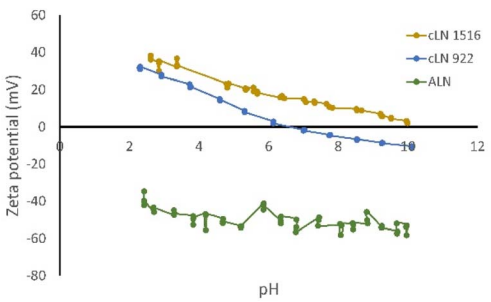

Fig. 2 Zeta potential measured across a range of pH values for aLN, cLN 922, and cLN 1516 mol% cationized lignin.

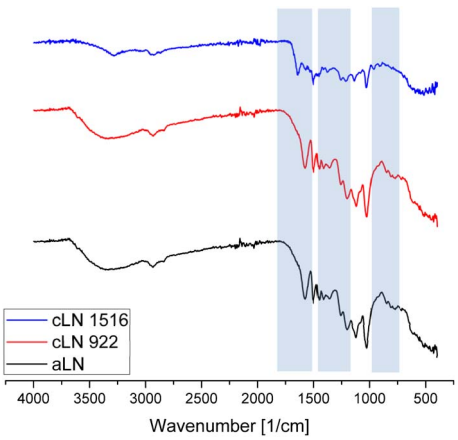

Fig. 3 Stacked FTIR spectra of unmodified and cationized lignin modifications cLN 922 mol% and 1516 mol%.

 © 2024 The Author(s). Published by the Royal Society of Chemistry

Open Access Article. Published on 30 September 2024. Downloaded on 10/24/2025 11:24:44 PM.
This article is licensed under a Creative Commons Attribution-NonCommercial 3.0 Unported Licence.

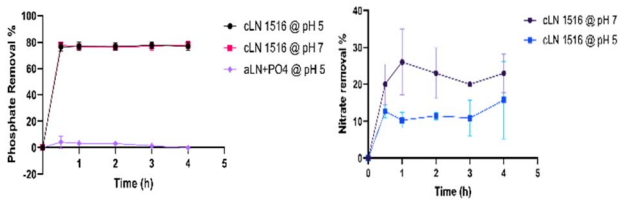

Fig. 4 Phosphate (left) and nitrate (right) adsorption by aLN at pH 5, and by cLN 1516 at pH 5 and 7.

−10.4 mV at pH 10.1, and the point of zero charge was at pH 6.6. For cLN 1516, the zeta potential ranged from +38.2 mV at pH 2.6 to 2.1 mV at pH 10.0, and the pH_{pzc} was not attained within this range (Fig. 2).

The fact that the surface charge of cLN 1516 remains positive shows that there was no pH environment where the surface charge of the adsorbent was neutralized and therefore would remove the adsorbate over a wide pH range. The zeta potential of the unmodified aLN was ≈ −44 at neutral pH and showing that the chemical modification of the lignin was successful. Hence, it was concluded that the charge of the cLN resulting from GTAC derivatization is permanent and not pH dependent, as later confirmed by the FTIR (Fig. 3); this is consistent with conclusions drawn in similar research by Wahlström.[20]

3.2.2. FT-IR analysis. FTIR analysis of the cLN (922 and 1516 mol%) compared to the unmodified aLN revealed the presence of new peaks (Fig. 3). Peak assignments for the FTIR spectra were referenced from Pinto[27] and Wang.[43] The broad peak at 3333 cm^{-1} is assigned to O–H stretching in the aliphatic and phenolic compounds, with an enhanced intensity in the cLN due to an increase in aliphatic OH groups from the opening of the epoxy ring. The peaks at 2939 cm^{-1} and 2840 cm^{-1} represent the C–H vibration of the methyl and methoxy groups, respectively.

Absorption peaks at 1583 cm^{-1} in both lignin types are attributed to the C–H vibration of the aromatic ring. This illustrates the existence of the aromatic skeletal structure in both lignin types. The appearance of new absorption peaks at 1465 cm^{-1} in cLN 1516 was attributed to the stretching of the symmetric-CH_3 in the quaternary ammonium compounds,[42] while the IR peaks at 968 cm^{-1}, and 910 cm^{-1} for the cLN are assigned to methyl and methylene groups linked to quaternary ammonium atoms.[27] This further demonstrates the successful grafting of GTAC on lignin, similar to Kong[30] who studied the cationization of kraft lignin. Furthermore, the peak at 1653 cm^{-1} in the cLN reflects the N–H bending in the ammonium salt, while the peak at 814 cm^{-1} is attributed to C–H deformations out-of-plane in positions 2 and 6 of the syringyl units.

3.3. Phosphate and nitrate adsorption

3.3.1. Effect of lignin cationization on adsorption. The phosphate and nitrate adsorption removal percentages with cLN 1516 at pH 5 and 7 compared to that of aLN at pH 5 are shown in Fig. 4. These pH values were selected to fall within the range of the pH of final effluents. The high removal rate of phosphate by cLN (∼80%) can be explained by the electrostatic interaction between the phosphates and the positively charged surface of the cLN which would be enhanced by the further protonation of the surface OH-groups in an acidic medium. We found no difference in adsorption at the two pH values investigated for phosphates. On the other hand, the phosphate adsorption by the unmodified aLN was less than 1% after 4 hours which could be explained by the electrostatic repulsion between the negatively charged aLN surface and the phosphates. Nitrate removal with cLN 1516 at the two pH environments revealed a rather different trend as shown in Fig. 4 right. Higher nitrate removal was achieved at pH 7. This could be explained by the nitrate speciation; in aqueous media, it exists as the NO_3^- and can be protonated at a lower pH decreasing its availability for adsorption, unlike at a higher pH. A similar trend was observed by Berkessa,[4] who suggested that it might be due to the aqueous phase pH governing the dissociation of active sorbent binding sites.

Based on these removal rates and titration results, cLN 1516, which conserved a positive charge within the target pH range of final effluent discharges,[6–8] was selected as the lignin modification for further adsorption experiments in the study.

3.3.2. Kinetic models and adsorption isotherms. Kinetic models and adsorption isotherms are used to describe the mechanism of adsorption and quantity of target adsorbate trapped onto the surface of the material per unit weight, under equilibrium conditions and at a constant temperature.[44] Among

Table 3 Isotherm and kinetic parameters for phosphate and nitrate removal

	Isotherms				Kinetics			
	Langmuir		Freundlich		PFO		PSO	
Adsorbate	Parameter	Value	Parameter	Value	Parameter	Value	Parameter	Value
Nitrates	q_{max} (mg g^{-1})	2	K_F	0.26	q_e (mg g^{-1})	0.82	q_e (mg g^{-1})	0.82
	K_L (mL mg^{-1})	0.09	$1/n$	0.53	$q_{e,cal}$ (mg g^{-1})	0.23	$q_{e,cal}$ (mg g^{-1})	0.67
	R_L	0.92	R^2	0.78	K_1 (min^{-1})	-4.18×10^{-6}	K_2 (g (mg min^{-1})$^{-1}$)	0.13
	R^2	0.84			R^2	0.05	R^2	0.99
Phosphates	q_{max} (mg g^{-1})	0.59	K_F	0.56	q_e (mg g^{-1})	0.25	q_e (mg g^{-1})	0.25
	K_L (mL mg^{-1})	2.87	$1/n$	0.6	$q_{e,cal}$ (mg g^{-1})	0.05	$q_{e,cal}$ (mg g^{-1})	0.22
	R_L	0.26	R^2	0.95	K_1 (min^{-1})	-7.97×10^{-5}	K_2 (g (mg min^{-1})$^{-1}$)	5.05
	R_2	0.97			R^2	0.6	R^2	1

Open Access Article. Published on 30 September 2024. Downloaded on 10/24/2025 11:24:44 PM.
This article is licensed under a Creative Commons Attribution-NonCommercial 3.0 Unported Licence.

Table 4 Phosphates and nitrates adsorption capacities and adsorbent dosages reported in the literature

Adsorbent material	Adsorption capacity (mg g^{-1})		Adsorbent dosage (mg mL^{-1})	Reference
	PO_4^{3-}	NO_3^-		
Mg–Fe oxide	28.3	NA	NA	46
Local clay	NA	5.1	20	3
Lanthanum-modified platanus biochar	148.11		0.4	47
Hybrid hydrated metal oxides				
HFeO	−111	NA	NA	48
HZrO	−92			
HCuO	−74			
Lanthanum-incorporated porous zeolite	17.2	NA	2	49
AL–PEI–La	65.79	NA	1.25	23
Tablet precipitation material (used cement)	3.81	NA	15	50
Solid waste residue (SWR) generated from Awash Melkassa Aluminium Sulphate and Sulphuric Acid Factory	0.962	0.071	20	4
Raw corn stalks (RCS)	22.8833	13.6054	1	38
Hybrid anion exchange (HA520E-Fe)	12.45	58.6	1	51
La-biochar	36.06	NA	2	52
Amorphous lanthanum hydroxide	107.53	NA	2.5	53
Nanosize-dispersed ZrO_2 particles on zirconia-functionalized graphite oxide (ZrAGO)	131.6	NA	0.5	54
Mg oak biochar (*in situ*)	64.6	NA	NA	55
Mg GHW biochar (*in situ*)	65.1	NA	NA	55
MgO-functionalized lignin-based bio-charcoal (MFLC)	295.91	NA	2	35
Zirconium(IV) loaded lignocellulosic butanol residue (LBR-Zr)	8.75	NA	NA	24
Hydrous zirconium oxide-based nanocomposite HZO-201	28	NA	0.5	56
Magnetic bio-activated carbons (MBACs)	21.18	NA	6.67	57
Magnetic lignin-based nanoparticles (M/ALFe)	0.09	NA	20	13
Dolomite	0.30	NA	60	45
Hydroxyapatite	1.10	NA	20	45
Fe_2O_3-contained lignocellulose nanocomposite	NA	26.12	4	10
Polymeric adsorbent (NDQ)	NA	221.8	2	2
Pyrolyzed biochar	NA	35.59	200	58
B/Mg400	138	NA	16.6	59
Cationic alkaline lignin (present study)	0.59	2	2	Present study

the Langmuir and Freundlich isotherms used to describe the isotherms, the Langmuir isotherm was found to describe phosphate and nitrate adsorption better, with R^2 values of 0.97 and 0.84 respectively (Table 3), indicating monolayer adsorption on a homogenous surface. In addition, the values of the separation factor R_L, which describes the nature of adsorption, were 0.26 and 0.92 respectively, and fall within the range $0 < R_L < 1$ indicating that the adsorption process was favorable[4,39] under these specific conditions. Comparing the K_L values, a higher value for the phosphates indicated a stronger adsorbent affinity for the phosphates than for nitrates. We also noticed that for phosphates, the data fit the Freundlich isotherm model with an R^2 of 0.95 suggesting that both homogenous and heterogeneous adsorbent surfaces were involved in phosphate adsorption. Similar results were reported by ref. 4 using solid waste residue for the simultaneous removal of phosphates and nitrates.

We assessed the pseudo-first- and second-order kinetic models with cLN 1516 at room temperature and neutral pH. The adsorption process was fast over the first 30 minutes but then flattened, possibly due to the saturation of adsorption sites. The adsorption kinetics revealed that phosphate and nitrate sorption onto cLN was better described by the pseudo-second-order model, which had a correlation coefficient close to unity as shown in Table 3. This was further supported by the fact that the estimated q_e values were close to the experimentally determined $q_{e,cal}$ values. Hence, the adsorption process was governed by electron exchange on the adsorbent surface with the adsorbate (chemisorption).

The adsorption capacities for phosphates and nitrates by various materials modified under various conditions is summarized in Table 4. The adsorbents that have not been modified with inorganic metallic components[3,4,45] display comparable adsorption capacities in the same range as our cationic lignin. The advantage of our system is that these adsorption capacities were obtained at only 2 mg mL^{-1} adsorbent dosage. This demonstrates the feasibility of the application of the proposed material for tertiary-stage wastewater treatment and the potential as a plant fertilizer source following the circular economy approach. With optimization, the adsorption capacities can be attained as shown in Section 3.3.3.

3.3.3. Effects of cLN adsorbent dose and initial adsorbate concentration. Doehlert's design allowed for the modeling and

 © 2024 The Author(s). Published by the Royal Society of Chemistry

Open Access Article. Published on 30 September 2024. Downloaded on 10/24/2025 11:24:44 PM.
This article is licensed under a Creative Commons Attribution-NonCommercial 3.0 Unported Licence.

Table 5 2-parameter Doehlert matrix for adsorbent dose and ion concentration, and resulting removal percentages

	Phosphates			Nitrates	
Exp't #	Ads dose (mg mL^{-1})	Conc. (mg L^{-1})	Removal%	Conc. (mg L^{-1})	Removal%
1	6	50.25	10.30 ± 2.37	13.6	32.10 ± 3.13
2	10	50.25	24.93 ± 0.94	13.6	52.40 ± 7.83
3	2	50.25	4.76 ± 1.57	13.6	13.28 ± 2.61
4	8	100.00	10.26 ± 0.18	24.1	28.42 ± 3.23
5	4	0.50	82.91 ± 0.76	3.0	35.00 ± 2.36
6	8	0.50	90.06 ± 3.28	3.0	76.67 ± 4.71
7	4	100.00	0.92 ± 0.31	24.1	21.78 ± 2.64

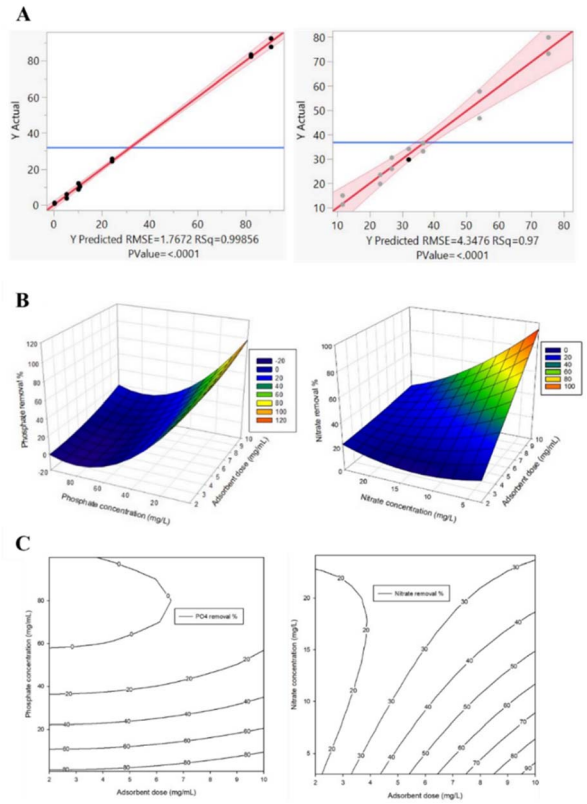

Fig. 5 (A) Actual *vs.* predicted responses; (B) effect of adsorbent dose and initial concentrations on removal percentage; (C) contour plots for phosphate and nitrate adsorption according to Doehlert's experimental design.

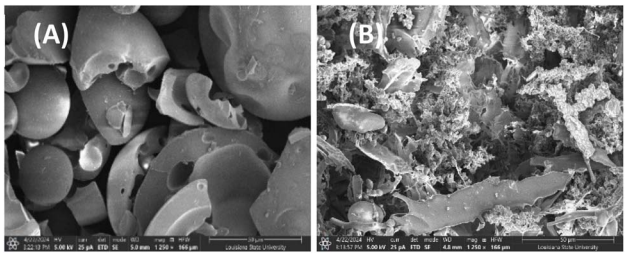

Fig. 6 SEM imaging at 1250× magnification of (A) aLN and (B) cLN 1516.

detection of the interaction between the studied parameters (adsorbent dose and ion concentration) and their effects on the response (removal percentage) using cLN 1516. Each adsorption experiment was carried out at pH 7 to reflect realistic WWTP effluent conditions and the contact time was kept constant at 25 min. As expected, the highest adsorbent dose had the highest removal rate for the lowest phosphate and nitrate concentrations (Table 5).

Multiple regression analysis applied to the experimental data showed that the model was statistically significant with *p*-values less than 0.05 (Table 5) for both phosphates and nitrates. The following equations were generated to represent phosphates (eqn (9)) and nitrates (eqn (10)) removal percentages:

$$Y_P = 84.12 - 1.31X_1 - 2.25X_2 + 0.28X_1^2 + 0.01X_2^2 + 0.01X_1X_2 \quad (9)$$

Table 6 Model coefficients and corresponding significance values estimated by regression analyses

	Phosphates			Nitrates		
Parameter	Coefficient	STD error	*p*-Value	Coefficient	STD error	*p*-Value
Intercept	84.12	3.874	2.13×10^{-8}	1.62	11.266	0.8894
X_1	−1.31	1.204	0.3066	10.34	3.0241	0.0091[a]
X_2	−2.25	0.061	3.29×10^{-10}[a]	−0.96	0.8277	0.2804
X_1^2	0.28	0.096	0.0179[a]	0.05	0.2353	0.8495
X_2^2	0.01	5×10^{-4}	1.59×10^{-9}[a]	0.07	0.0254	0.0200[a]
X_1X_2	0.01	0.006	0.4074	−0.42	0.0728	0.0005[a]
Overall *p*-value	3.87×10^{-11}			4.86×10^{-6}		
Adjusted R^2	1			0.96		

[a] Significant at $p < 0.05$.

Open Access Article. Published on 30 September 2024. Downloaded on 10/24/2025 11:24:44 PM.
This article is licensed under a Creative Commons Attribution-NonCommercial 3.0 Unported Licence.

$$Y_N = 1.62 + 10.34X_1 - 0.96X_2 + 0.05X_1^2 + 0.07X_2^2 - 0.42X_1X_2 \quad (10)$$

Clustering points around the diagonal indicate a good fit and validate the model with the plot of predicted *versus* experimental values[60] for both phosphates and nitrates (Fig. 5A) with regression coefficient R^2 values of 1.00 and 0.97 respectively.

The significance of the model coefficients at the 95% confidence interval was determined using the Student's *t*-test as

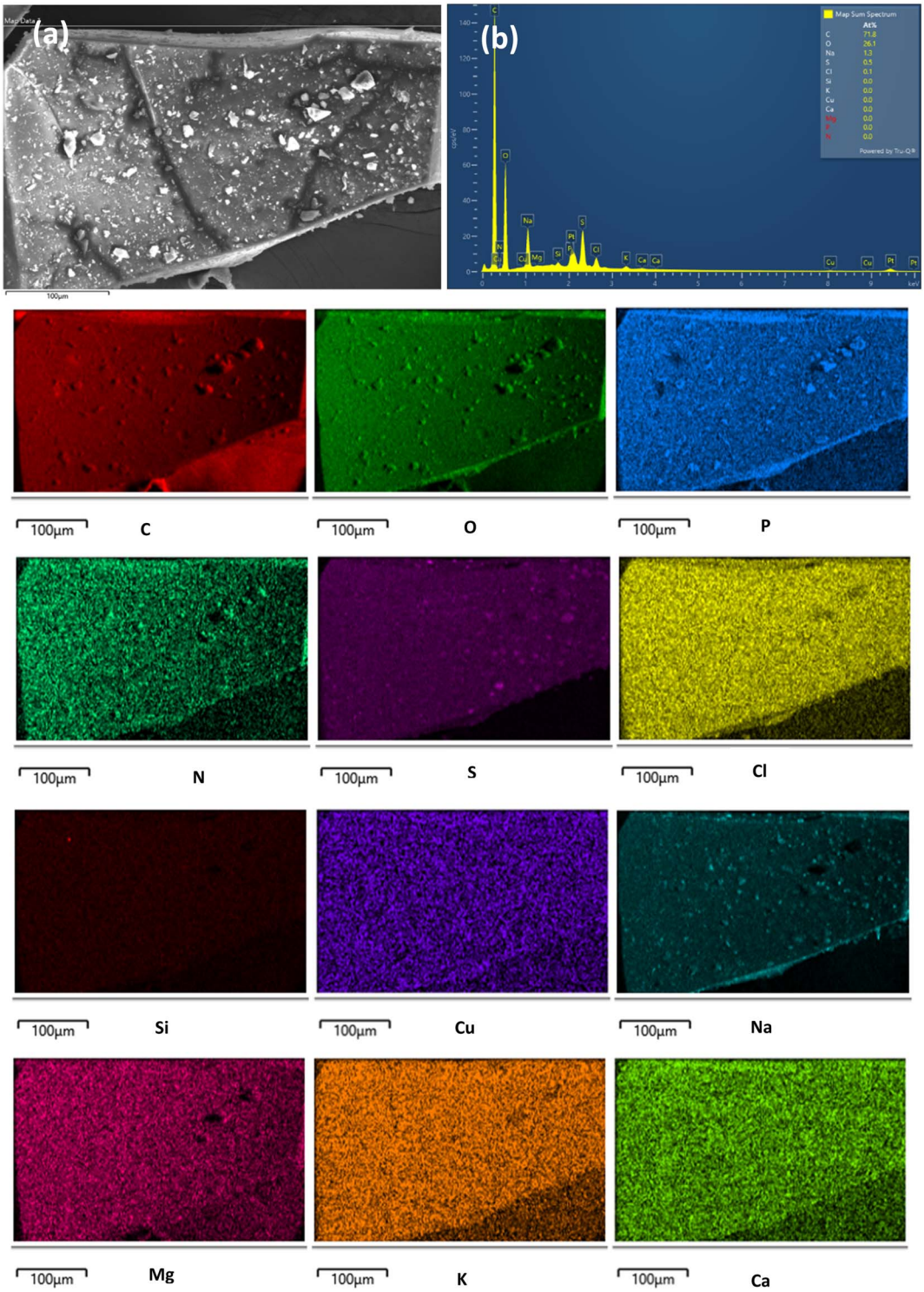

Fig. 7 SEM/EDS image of elemental mapping of cLN 1516 after adsorption showing (a) electron image and (b) area EDS spectrum of the labelled elements.

 © 2024 The Author(s). Published by the Royal Society of Chemistry

Open Access Article. Published on 30 September 2024. Downloaded on 10/24/2025 11:24:44 PM.
This article is licensed under a Creative Commons Attribution-NonCommercial 3.0 Unported Licence.

summarized in Table 6. On the one hand, the interaction between the adsorbent dose and phosphate concentration is insignificant. However, the phosphate concentration is significant in the first and second order, while the adsorbent dose is only significant at the second order. This means that the adsorbent dose does not affect phosphate removal significantly when considered linearly unlike the phosphate concentration where a small variation would influence the phosphate removal considerably. On the other hand, the interaction between the adsorbent dose and nitrate concentration is significant. Variations in adsorbent dose would affect the nitrate removal considerably when considered linearly but not at the second-order level. The nitrate concentration is significant only at the second-order level.

From the response surface plots, it can be deduced that adsorption sites reached saturation quickly, with little or no adsorbate retention as the exchange sites were overwhelmed (Fig. 5B). Exploiting the vicinity of optimum from the contour plots (Fig. 5C), the optimum conditions for phosphate removal were an adsorbent dose of 5 mg mL^{-1} and a phosphate concentration of 0.5 mg L^{-1} while the corresponding optimum conditions for nitrates were 10 mg mL^{-1} and 4.1 mg L^{-1}. The theoretical removal percentages corresponding to these optimum points for phosphates and nitrates were 83.54% and 89.94% respectively while the experimental removal percentages were 92.66% and 80.95% respectively. After verification, the percentage difference between the theoretical and experimental data for phosphates was 9.842% and for nitrates was 9.996%. The fact that both differences were <10% validated the model and further confirmed that cLN 1516 mol% is highly effective at low phosphate and nitrate concentrations with adsorption capacities of 1.15 mg g^{-1} and 8.5 mg g^{-1}. Since our target is final effluent, which usually has lower ion concentrations after primary and secondary treatments (TN: 15–35 mg L^{-1} and TP: 4–10 mg L^{-1}),[1] our cLN functions well within that range as a tertiary treatment but would not be effective for systems with higher concentrations.

3.3.4. Treatment of South Baton Rouge (SBR) WWTP effluent. The SBR WWTP was built in 1958 and upgraded in 2018 with a design capacity of 205 million gallons of wastewater and employs an additional layer of treatment using an aeration tank. After treatment, the water from the plant is discharged into the Mississippi River. The estimated phosphate concentrations of the final effluent of the first set of samples collected from SBR WWTPs was 0.42 mg L^{-1}, while nitrate concentration was 4.1 mg L^{-1}. Their corresponding native pH was 6.37. According to the United States Environmental Protection Agency (USEPA), before discharging into receiving waters, WWTP effluent concentrations of total phosphorus (TP) and total nitrogen (TN) should be maintained below 0.2 mg L^{-1} and 2 mg L^{-1} respectively.[61,62]

Results from the adsorption experiments carried out on the SBR WWTP using the experimentally determined (see Section 3.3.3) optimum adsorbent dose of 10 mg mL^{-1} showed a significant reduction of nutrient loads of 57.7% and 43.9% for phosphates and nitrates respectively. These effluent samples, present contain several types of pollutants such as chlorides, sulfates, and carbonates at varied concentrations; they probably competed with phosphates and nitrates for the adsorption sites, thereby limiting the adsorption of the phosphates and nitrates to the observed 57.7% and 43.9%. We could not report the averages because the subsequent set of SBR WWTP samples collected had low initial phosphate and nitrate concentrations (0.03 mg L^{-1} and 0.67 mg L^{-1} respectively) and were below detection limits after adsorption. This aligns with conclusions from the Doehlert experiments that the lower the concentration, the higher the removal percentage.

3.4. Morphological and elemental analysis

SEM imaging of aLN (Fig. 6A) and cLN 1516 (Fig. 6B) was performed to highlight their characteristic morphological differences. Compared to aLN, cLN 1516 had more irregular, porous, and random shapes with more available surfaces for interaction with adsorbates.

Elemental mapping by SEM/EDS of the adsorbent after adsorption revealed its surface elemental composition (Fig. 7). As expected, the typical chemical constituent elements in wastewater as reported by Chang's group[63] are present on the adsorbent surface displayed by the EDS mapping. Most of these elements (Ca, Mg, Na, K, S) are common in the natural environment while trace elements such as Cu come from domestic wastewater. The confirmation of the presence of other anions on the adsorbent surface further confirms that they compete for adsorption sites thereby limiting the adsorption of phosphates and nitrates.

4. Conclusions

High nutrient loads of wastewater treatment plant effluents released into natural waters hinder the attainment of water quality standards. In our study, alkaline lignin was chemically modified to provide the positive charge needed for removing anionic pollutants from wastewater. The structure of the functionalized lignin polymer was confirmed with NMR, FTIR, and SEM/EDS. The most promising cationic lignin modification variant was further tested in adsorption experiments to determine its efficacy for removing phosphates and nitrates from wastewater. Nitrates and phosphates were chosen because not only they are predominant pollutants in effluents from water treatment plants but also macronutrients that can be applied as fertilizers after removal. A 2-dimensional Doehlert matrix was used to model the effects of initial concentration and adsorbent dose on phosphate and nitrate removal, and we showed that cLN 1516 was most effective at low phosphate and nitrate concentrations. With an experimentally determined optimum adsorbent dose of 10 mg mL^{-1}, we reduced nutrient loads with removal of 57.7% and 43.9% for phosphates and nitrates respectively. Our research demonstrates that lignin, a byproduct of the pulp and paper industry, can be repurposed as a wastewater remediation material with possible application as a plant nutrient source, thereby closing the circular economy loop.

Open Access Article. Published on 30 September 2024. Downloaded on 10/24/2025 11:24:44 PM.
This article is licensed under a Creative Commons Attribution-NonCommercial 3.0 Unported Licence.

Data availability

Data for this article, including tables of phosphate and nitrate kinetics, isotherms, Doehlert's matrix design, and adsorption data are available at Science Data Bank at https://doi.org/10.57760/sciencedb.09760.

Conflicts of interest

There are no conflicts to declare.

Acknowledgements

We thank Thomas P. Blanchard of the Department of Oceanography and Coastal Sciences, College of the Coast and Environment, Louisiana State University for his help and guidance with the phosphate measurement protocols. We thank Dr Dorin Boldor and Dr Yongchan Kwon of the Biological & Agricultural Engineering Department, Louisiana State University for permission to use their centrifuge. We thank Dr Chandra Theegala of the Biological & Agricultural Engineering Department, Louisiana State University for his assistance with the spectrophotometer. We also thank Mr Michael Lowe and Ms Cynthia Thomas, both wastewater treatment lab supervisors, for their help with wastewater samples and characteristic data. We also acknowledge financial support from the Louisiana Board of Regents and the USDA NIFA.

References

1 R. O. Carey and K. W. Migliaccio, Contribution of wastewater treatment plant effluents to nutrient dynamics in aquatic systems, *Environ. Manage.*, 2009, **44**(2), 205–217.
2 Y. Wu, Y. Wang, J. Wang, S. Xu, L. Yu, C. Philippe, *et al.*, Nitrate removal from water by new polymeric adsorbent modified with amino and quaternary ammonium groups: batch and column adsorption study, *J. Taiwan Inst. Chem. Eng.*, 2016, **66**, 191–199, DOI: 10.1016/j.jtice.2016.06.019.
3 A. Battas, A. El Gaidoumi, A. Ksakas and A. Kherbeche, Adsorption study for the removal of nitrate from water using local clay, *Sci. World J.*, 2019, **2019**, 1–10, DOI: 10.1155/2019/9529618.
4 Y. W. Berkessa, S. T. Mereta and F. F. Feyisa, Simultaneous removal of nitrate and phosphate from wastewater using solid waste from factory, *Appl. Water Sci.*, 2019, **9**(2), 1–10, DOI: 10.1007/s13201-019-0906-z.
5 T. Wu, S. S. Yang, L. Zhong, J. W. Pang, L. Zhang, X. F. Xia, *et al.*, Simultaneous nitrification, denitrification and phosphorus removal: what have we done so far and how do we need to do in the future?, *Sci. Total Environ.*, 2023, **856**, 158977, DOI: 10.1016/j.scitotenv.2022.158977.
6 F. Mahoo, Methods for phosphorus recovery from waste water: a review, *J. Biodiversity Environ. Sci.*, 2018, **13**(2), 315–323.
7 A. Bhatnagar and M. Sillanpää, A review of emerging adsorbents for nitrate removal from water, *Chem. Eng. J.*, 2011, **168**(2), 493–504, DOI: 10.1016/j.cej.2011.01.103.
8 J. Xie, Z. Wang, S. Lu, D. Wu, Z. Zhang and H. Kong, Removal and recovery of phosphate from water by lanthanum hydroxide materials, *Chem. Eng. J.*, 2014, **254**, 163–170.
9 A. A. Werkneh and E. R. Rene, Applications of Nanotechnology and Biotechnology for Sustainable Water and Wastewater Treatment, *Energy Environ. Sustainability*, 2019, 405–430.
10 S. Abdolmaleki, S. M. Amininasab and M. Ghadermazi, Modification of Fe_2O_3-contained lignocellulose nanocomposite with silane group to remove nitrate and bacterial contaminations from wastewater, *Iran. Polym. J.*, 2019, **28**(10), 859–872, DOI: 10.1007/s13726-019-00749-9.
11 N. Öztürk and T. E. Bektaş, Nitrate removal from aqueous solution by adsorption onto various materials, *J. Hazard. Mater.*, 2004, **112**(1–2), 155–162.
12 M. Sajjadi, F. Ahmadpoor, M. Nasrollahzadeh and H. Ghafuri, Lignin-derived (nano)materials for environmental pollution remediation: current challenges and future perspectives, *Int. J. Biol. Macromol.*, 2021, **178**, 394–423, DOI: 10.1016/j.ijbiomac.2021.02.165.
13 T. Li, S. Lü, Z. Wang, M. Huang, J. Yan and M. Liu, Lignin-based nanoparticles for recovery and separation of phosphate and reused as renewable magnetic fertilizers, *Sci. Total Environ.*, 2021, **765**, 142745, DOI: 10.1016/j.scitotenv.2020.142745.
14 D. Wang, S. H. Lee, J. Kim and C. B. Park, "Waste to Wealth": Lignin as a Renewable Building Block for Energy Harvesting/Storage and Environmental Remediation, *ChemSusChem*, 2020, **13**(11), 2807–2827.
15 J. G. Lee, L. L. Larive, K. T. Valsaraj and B. Bharti, Binding of Lignin Nanoparticles at Oil-Water Interfaces: An Ecofriendly Alternative to Oil Spill Recovery, *ACS Appl. Mater. Interfaces*, 2018, **10**(49), 43282–43289.
16 Q. Tang, Y. Qian, D. Yang, X. Qiu and Y. Qin, Lignin-Based Nanoparticles: A Review on Their Preparations and Applications, *Polymers*, 2020, 12–16.
17 L. Hu, C. Guang, Y. Liu, Z. Su, S. Gong, Y. Yao, *et al.*, Adsorption behavior of dyes from an aqueous solution onto composite magnetic lignin adsorbent, *Chemosphere*, 2020, **246**, 125757, DOI: 10.1016/j.chemosphere.2019.125757.
18 H. W. Kwak, H. Lee and K. H. Lee, Surface-modified spherical lignin particles with superior Cr(VI) removal efficiency, *Chemosphere*, 2020, **239**, 124733, DOI: 10.1016/j.chemosphere.2019.124733.
19 A. Naseer, A. Jamshaid, A. Hamid, N. Muhammad, M. Ghauri, J. Iqbal, *et al.*, Lignin and lignin based materials for the removal of heavy metals from waste water - an overview, *Z. Phys. Chem.*, 2019, **233**(3), 315–345.
20 R. Wahlström, A. Kalliola, J. Heikkinen, H. Kyllönen and T. Tamminen, Lignin cationization with glycidyltrimethylammonium chloride aiming at water purification applications, *Ind. Crops Prod.*, 2017, **104**(February), 188–194, DOI: 10.1016/j.indcrop.2017.04.026.
21 H. Guo, Y. Chen, S. Yang, R. Li, X. Zhang, Q. Dong, *et al.*, Lignin-based adsorbent-catalyst with high capacity and stability for polychlorinated aromatics removal, *Bioresour.*

 © 2024 The Author(s). Published by the Royal Society of Chemistry

Open Access Article. Published on 30 September 2024. Downloaded on 10/24/2025 11:24:44 PM.
This article is licensed under a Creative Commons Attribution-NonCommercial 3.0 Unported Licence.

Technol., 2021, **337**(June), 125453, DOI: 10.1016/j.biortech.2021.125453.

22 T. Zhao, K. Zhang, J. Chen, X. Shi, X. Li, Y. Ma, *et al.*, Changes in heavy metal mobility and availability in contaminated wet-land soil remediated using lignin-based poly(acrylic acid), *J. Hazard. Mater.*, 2019, **368**(January), 459–467.

23 E. Zong, G. Huang, X. Liu, W. Lei, S. Jiang, Z. Ma, *et al.*, A lignin-based nano-adsorbent for superfast and highly selective removal of phosphate, *J. Mater. Chem. A*, 2018, **6**(21), 9971–9983, available from: http://xlink.rsc.org/?DOI=C8TA01449C.

24 E. Zong, X. Liu, J. Jiang, S. Fu and F. Chu, Preparation and characterization of zirconia-loaded lignocellulosic butanol residue as a biosorbent for phosphate removal from aqueous solution, *Appl. Surf. Sci.*, 2016, **387**, 419–430, DOI: 10.1016/j.apsusc.2016.06.107.

25 P. Ekins, T. Domenech, P. Drummond, R. Bleischwitz, N. Hughes and L. Lotti, The Circular Economy: What, Why, How and Where, *Managing Environmental and Energy Transitions for Regions and Cities*, 2019, pp. 1–89, available from: https://www.oecd.org/cfe/regionaldevelopment/Ekins-2019-Circular-Economy-What-Why-How-Where.pdf.

26 H. Gogoi, T. Leiviskä, J. Rämö and J. Tanskanen, Production of aminated peat from branched polyethylenimine and glycidyltrimethylammonium chloride for sulphate removal from mining water, *Environ. Res.*, 2019, **175**(January), 323–334, DOI: 10.1016/j.envres.2019.05.022.

27 P. I. F. Pinto, S. Magina, E. Budjav, P. C. R. Pinto, F. Liebner and D. Evtuguin, Cationization of Eucalyptus Kraft LignoBoost Lignin: Preparation, Properties, and Potential Applications, *Ind. Eng. Chem. Res.*, 2022, **61**(10), 3503–3515.

28 S. Chauhan, B. Kumari, G. S. Chauhan, K. Chauhan, S. Ranote, R. Kumar, *et al.*, A highly efficient and green adsorbent for anionic dyes synthesized from whole pine needles modified with glycidyltrimethylammonium chloride: synthesis, kinetic, and thermodynamic investigation, *Biomass Convers. Biorefin.*, 2023, **1**, 3, DOI: 10.1007/s13399-023-04776-8.

29 H. Zhang, K. Xue, B. Wang, W. Ren, D. Sun, C. Shao, *et al.*, Advances in lignin-based biosorbents for sustainable wastewater treatment, *Bioresour. Technol.*, 2024, **395**(January), 130347, DOI: 10.1016/j.biortech.2024.130347.

30 F. Kong, K. Parhiala, S. Wang and P. Fatehi, Preparation of cationic softwood kraft lignin and its application in dye removal, *Eur. Polym. J.*, 2015, **67**, 335–345, DOI: 10.1016/j.eurpolymj.2015.04.004.

31 D. S. Argyropoulos, N. Pajer and C. Crestini, Quantitative ^{31}P NMR Analysis of Lignins and Tannins, *J. Visualized Exp.*, 2021, **174**, e62696, DOI: 10.3791/62696.

32 A. Granata and D. S. Argyropoulos, 2-Chloro-4,4,5,5-tetramethyl-1,3,2-dioxaphospholane, a Reagent for the Accurate Determination of the Uncondensed and Condensed Phenolic Moieties in Lignins, *J. Agric. Food Chem.*, 1995, 1538–1544.

33 X. Meng, C. Crestini, H. Ben, N. Hao, Y. Pu, A. J. Ragauskas, *et al.*, Determination of hydroxyl groups in biorefinery resources via quantitative ^{31}P NMR spectroscopy, *Nat. Protoc.*, 2019, **14**(9), 2627–2647, DOI: 10.1038/s41596-019-0191-1.

34 J. F. Araneda, I. W. Burton, M. Paleologou, S. D. Riegel and M. C. Leclerc, Analysis of lignins using ^{31}P benchtop NMR spectroscopy: quantitative assessment of substructures and comparison to high-field NMR, *Can. J. Chem.*, 2022, **100**(11), 799–808.

35 G. J. Jiao, J. Ma, Y. Li, D. Jin, Y. Guo, J. Zhou, *et al.*, Enhanced adsorption activity for phosphate removal by functional lignin-derived carbon-based adsorbent: optimization, performance and evaluation, *Sci. Total Environ.*, 2021, **761**, 143217, DOI: 10.1016/j.scitotenv.2020.143217.

36 S. L. C. Ferreira, W. N. L. Dos Santos, C. M. Quintella, B. B. Neto and J. M. Bosque-Sendra, Doehlert matrix: a chemometric tool for analytical chemistry - review, *Talanta*, 2004, **63**(4), 1061–1067.

37 C. Resendiz-Moctezuma, A. P. L. Fonville, B. N. Harsh, M. J. Stasiewicz and M. J. Miller, Use of Doehlert Matrix as a Tool for High-Throughput Screening of Organic Acids and Essential Oils on Miniaturized Pork Loins, Followed by Lab-Scale Validation That Confirmed Tested Compounds Do Not Show Synergistic Effects against Salmonella Typhimurium, *Foods*, 2023, **12**(21), 4034, DOI: 10.3390/foods12214034.

38 C. Fan and Y. Zhang, Adsorption isotherms, kinetics and thermodynamics of nitrate and phosphate in binary systems on a novel adsorbent derived from corn stalks, *J. Geochem. Explor.*, 2018, **188**(April 2017), 95–100, DOI: 10.1016/j.gexplo.2018.01.020.

39 P. Saha, S. Datta and S. K. Sanyal, Application of Natural Clayey Soil as Adsorbent for the Removal of Copper from Wastewater, *J. Environ. Eng.*, 2010, **136**(12), 1409–1417.

40 O. S. H. Santos, M. Coelho da Silva, V. R. Silva, W. N. Mussel and M. I. Yoshida, Polyurethane foam impregnated with lignin as a filler for the removal of crude oil from contaminated water, *J. Hazard. Mater.*, 2017, **324**, 406–413, DOI: 10.1016/j.jhazmat.2016.11.004.

41 K. Y. Foo and B. H. Hameed, Insights into the modeling of adsorption isotherm systems, *Chem. Eng. J.*, 2010, **156**(1), 2–10.

42 K. Acurio Cerda, M. Kathol, G. Purohit, E. Zamani, M. D. Morton, O. Khalimonchuk, *et al.*, Cationic Lignin as an Efficient and Biorenewable Antimicrobial Material, *ACS Sustainable Chem. Eng.*, 2023, **11**(28), 10364–10379, DOI: 10.1021/acssuschemeng.3c01414.

43 Y. Wang, W. Liu, L. Zhang and Q. Hou, Characterization and comparison of lignin derived from corncob residues to better understand its potential applications, *Int. J. Biol. Macromol.*, 2019, **134**, 20–27, DOI: 10.1016/j.ijbiomac.2019.05.013.

44 E. L. Ungureanu, A. L. Mocanu, C. A. Stroe, C. M. Panciu, L. Berca and R. M. Sionel, Agricultural Byproducts Used as Low-Cost Adsorbents for Removal of Potentially Toxic Elements from Wastewater: A Comprehensive Review, *Sustainability*, 2023, **15**(7), 5999, DOI: 10.3390/su15075999.

45 S. P. Boeykens, M. N. Piol, L. Samudio Legal, A. B. Saralegui and C. Vázquez, Eutrophication decrease: phosphate

Open Access Article. Published on 30 September 2024. Downloaded on 10/24/2025 11:24:44 PM.
This article is licensed under a Creative Commons Attribution-NonCommercial 3.0 Unported Licence.

adsorption processes in presence of nitrates, *J. Environ. Manage.*, 2017, **203**, 888–895.

46 Y. Xu, T. Liu, Y. Huang, J. Zhu and R. Zhu, Role of phosphate concentration in control for phosphate removal and recovery by layered double hydroxides, *Environ. Sci. Pollut. Res.*, 2020, **27**(14), 16612–16623.

47 Z. Jia, W. Zeng, H. Xu, S. Li and Y. Peng, Adsorption removal and reuse of phosphate from wastewater using a novel adsorbent of lanthanum-modified platanus biochar, *Process Saf. Environ. Prot.*, 2020, **140**, 221–232, DOI: 10.1016/j.psep.2020.05.017.

48 N. Y. Acelas, B. D. Martin, D. López and B. Jefferson, Selective removal of phosphate from wastewater using hydrated metal oxides dispersed within anionic exchange media, *Chemosphere*, 2015, **119**, 1353–1360.

49 Y. He, H. Lin, Y. Dong and L. Wang, Preferable adsorption of phosphate using lanthanum-incorporated porous zeolite: characteristics and mechanism, *Appl. Surf. Sci.*, 2017, **426**, 995–1004, DOI: 10.1016/j.apsusc.2017.07.272.

50 S. Yang, P. Jin, X. Wang, Q. Zhang and X. Chen, Phosphate recovery through adsorption assisted precipitation using novel precipitation material developed from building waste: behavior and mechanism, *Chem. Eng. J.*, 2016, **292**, 246–254, DOI: 10.1016/j.cej.2016.02.006.

51 S. Wiriyathamcharoen, S. Sarkar, P. Jiemvarangkul, T. T. Nguyen, W. Klysuban and S. Padungthon, Synthesis optimization of hybrid anion exchanger containing triethylamine functional groups and hydrated Fe(III) oxide nanoparticles for simultaneous nitrate and phosphate removal, *Chem. Eng. J.*, 2020, **381**(May 2019), 122671, DOI: 10.1016/j.cej.2019.122671.

52 Q. Xu, Z. Chen, Z. Wu, F. Xu, D. Yang, Q. He, *et al.*, Novel lanthanum doped biochars derived from lignocellulosic wastes for efficient phosphate removal and regeneration, *Bioresour. Technol.*, 2019, **289**(April), 121600, DOI: 10.1016/j.biortech.2019.121600.

53 J. Xie, Z. Wang, S. Lu, D. Wu, Z. Zhang and H. Kong, Removal and recovery of phosphate from water by lanthanum hydroxide materials, *Chem. Eng. J.*, 2014, **254**, 163–170, DOI: 10.1016/j.cej.2014.05.113.

54 E. Zong, D. Wei, H. Wan, S. Zheng, Z. Xu and D. Zhu, Adsorptive removal of phosphate ions from aqueous solution using zirconia-functionalized graphite oxide, *Chem. Eng. J.*, 2013, **221**, 193–203, DOI: 10.1016/j.cej.2013.01.088.

55 C. A. Takaya, L. A. Fletcher, S. Singh, U. C. Okwuosa and A. B. Ross, Recovery of phosphate with chemically modified biochars, *J. Environ. Chem. Eng.*, 2016, **4**(1), 1156–1165, DOI: 10.1016/j.jece.2016.01.011.

56 L. Chen, X. Zhao, B. Pan, W. Zhang, M. Hua, L. Lv, *et al.*, Preferable removal of phosphate from water using hydrous zirconium oxide-based nanocomposite of high stability, *J. Hazard. Mater.*, 2015, **284**, 35–42.

57 T. Han, X. Lu, Y. Sun, J. Jiang, W. Yang and P. G. Jönsson, Magnetic bio-activated carbon production from lignin via a streamlined process and its use in phosphate removal from aqueous solutions, *Sci. Total Environ.*, 2020, **708**, 135069, DOI: 10.1016/j.scitotenv.2019.135069.

58 S. Li, T. Galoustian and H. Trejo, Biochar pyrolyzed with concentrated solar radiation for enhanced nitrate adsorption, *J. Anal. Appl. Pyrolysis*, 2023, **174**(July), 106131, DOI: 10.1016/j.jaap.2023.106131.

59 M. de Carvalho Eufrásio Pinto, D. David da Silva, A. L. Amorim Gomes, R. M. Menezes dos Santos, R. A. Alves de Couto, R. Ferreira de Novais, *et al.*, Biochar from carrot residues chemically modified with magnesium for removing phosphorus from aqueous solution, *J. Cleaner Prod.*, 2019, **222**, 36–46.

60 S. B. Imandi, V. V. R. Bandaru, S. R. Somalanka and H. R. Garapati, Optimization of medium constituents for the production of citric acid from byproduct glycerol using Doehlert experimental design, *Enzyme Microb. Technol.*, 2007, **40**(5), 1367–1372.

61 H. Xu, H. W. Paerl, B. Qin, G. Zhu, N. S. Hall and Y. Wu, Determining critical nutrient thresholds needed to control harmful cyanobacterial blooms in eutrophic Lake Taihu, China, *Environ. Sci. Technol.*, 2015, **49**(2), 1051–1059.

62 Q. Zhou, H. Sun, L. Jia, W. Wu and J. Wang, Simultaneous biological removal of nitrogen and phosphorus from secondary effluent of wastewater treatment plants by advanced treatment: a review, *Chemosphere*, 2022, **296**(December 2021), 134054, DOI: 10.1016/j.chemosphere.2022.134054.

63 A. C. Chang, A. L. Page and F. T. Bingham, Re-utilization of municipal wastewater sludges - metals and nitrate, *J. Water Pollut. Control Fed.*, 1981, **53**(2), 237–245.

 © 2024 The Author(s). Published by the Royal Society of Chemistry